doi:10.1016/j.jmb.2011.03.004 J. Mol. Biol. (2011) 408, 555–567

Contents lists available at www.sciencedirect.com

Journal of Molecular Biology

journal homepage: http://ees.elsevier.com.jmb

Structural and Thermodynamic Effects of Post-translational Modifications in Mutant and Wild Type Cu, Zn Superoxide Dismutase

Elizabeth A. Proctor[1,2], Feng Ding[3,4] and Nikolay V. Dokholyan[1,2,3,4]*

[1]*Department of Biochemistry and Biophysics, University of North Carolina at Chapel Hill, School of Medicine, Chapel Hill, NC 27599, USA*
[2]*Program in Molecular and Cellular Biophysics, University of North Carolina at Chapel Hill, School of Medicine, Chapel Hill, NC 27599, USA*
[3]*Department of Biochemistry and Biophysics, University of North Carolina at Chapel Hill, School of Medicine, Chapel Hill, NC 27599, USA*
[4]*Center for Computational and Systems Biology, University of North Carolina at Chapel Hill, School of Medicine, Chapel Hill, NC 27599, USA*

Received 28 November 2010; received in revised form 25 February 2011; accepted 1 March 2011
Available online 9 March 2011

Edited by D. Case

Keywords:
amyotrophic lateral sclerosis; Cu,Zn superoxide dismutase; protein aggregation; post-translational modification; protein stability

Aggregation of Cu,Zn superoxide dismutase (SOD1) is implicated in amyotrophic lateral sclerosis. Glutathionylation and phosphorylation of SOD1 is omnipresent in the human body, even in healthy individuals, and has been shown to increase SOD1 dimer dissociation, which is the first step on the pathway toward SOD1 aggregation. We found that post-translational modification of SOD1, especially glutathionylation, promotes dimer dissociation. We discovered an intermediate state in the pathway to dissociation, a conformational change that involves a "loosening" of the β-barrels and a loss or shift of dimer interface interactions. In modified SOD1, this intermediate state is stabilized as compared to unmodified SOD1. The presence of post-translational modifications could explain the environmental factors involved in the speed of disease progression. Because post-translational modifications such as glutathionylation are often induced by oxidative stress, post-translational modification of SOD1 could be a factor in the occurrence of sporadic cases of amyotrophic lateral sclerosis, which represent 90% of all cases of the disease.

Introduction

The homodimeric metal-binding enzyme Cu,Zn superoxide dismutase (SOD1) is implicated in amyotrophic lateral sclerosis (ALS). Of all ALS cases, 10% are familial (fALS), and 20% of the fALS cases are attributed to mutations in SOD1.[1] Since the initial identification in 1993 of 11 different SOD1 mutants in patients with ALS,[2] researchers have linked over 100 point mutations throughout the length of this protein to fALS†.

Structurally, SOD1 is a cytosolic enzyme composed of two monomers of 153 residues each. Each monomer folds into a β-barrel formed of eight anti-

*Corresponding author. E-mail address: dokh@unc.edu.

Abbreviations used: SOD1, Cu,Zn superoxide dismutase; ALS, amyotrophic lateral sclerosis; fALS, familial ALS; MD, molecular dynamics; DMD, discrete molecular dynamics.

† http://alsod.iop.kcl.ac.uk

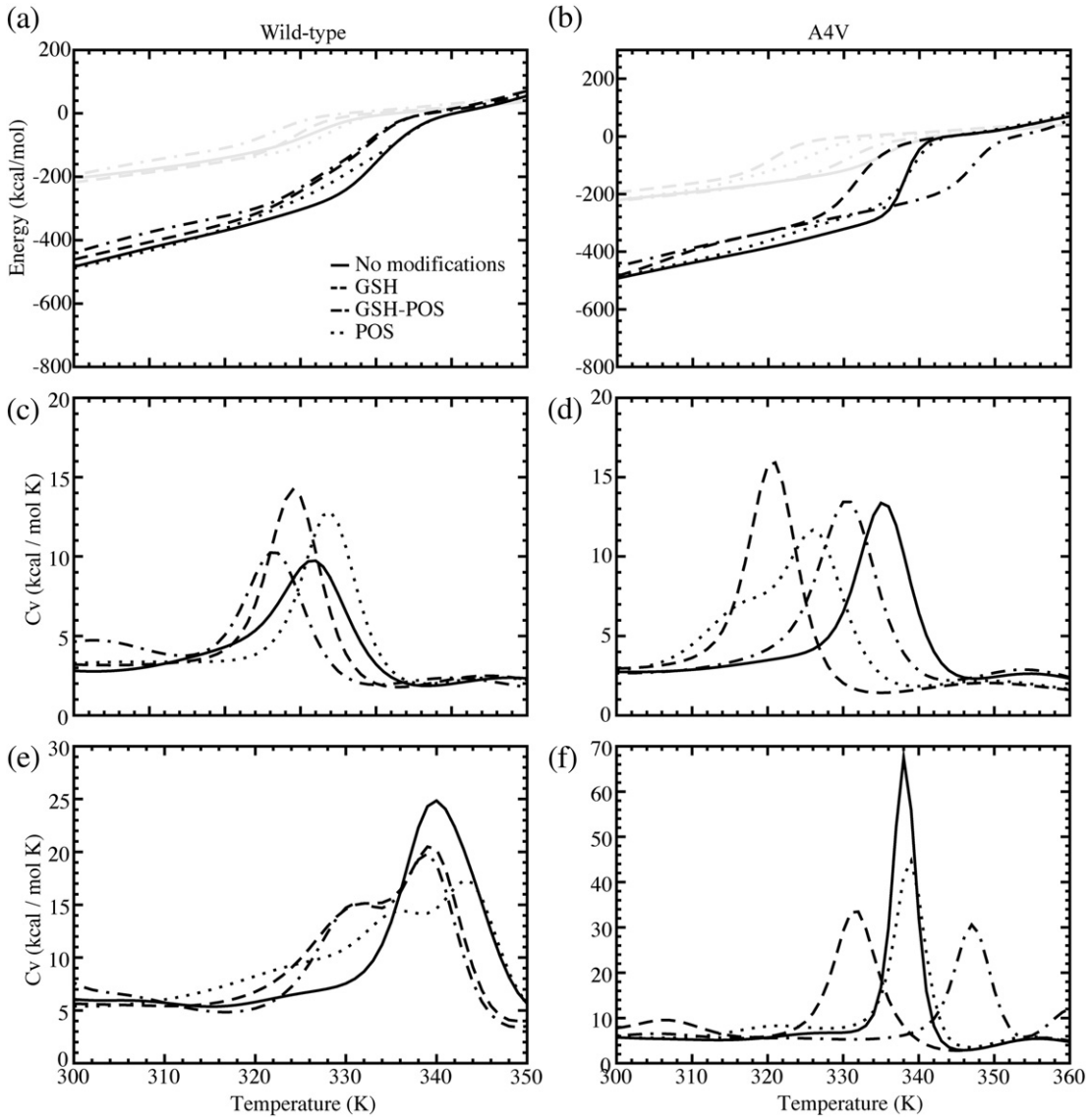

Fig. 1. Thermodynamics. Comparison of wild type (first column) and mutant A4V (second column) modified and unmodified SOD1. (a and b) Potential energy of the SOD1 complex according to the simulation temperature. Monomer curves are shown in gray and dimer curves are shown in black. (c and d) Specific heat as a function of temperature for the SOD1 monomer. (e and f) Specific heat as a function of temperature for the SOD1 dimer. Legends shown for the wild type are relevant also for A4V.

parallel strands configured in a Greek key formation.[3] Each monomer has two major loops, the electrostatic and zinc-binding loops, coordinated by the β-barrels.[4] These loops are coordinated by a zinc ion, which makes a large contribution to the stability of the dimer.[5,6] The dimer is also stabilized by a disulfide bond between cysteines 57 and 146, which connect the zinc-binding loop to the C-terminal β-strand.[7–9]The enzymatic activity of SOD1 is enabled by a copper ion, which dismutates superoxide ion to molecular oxygen and hydrogen peroxide.[10,11]

Although the exact mechanism of the progressive motor neuron death characteristic of ALS is still unknown, there is evidence that aggregates of SOD1 are the cytotoxic species.[12,13] The first step toward aggregation of SOD1 protein is hypothesized to be dissociation of the SOD1 dimer into monomers, followed by metal loss and unfolding.[5,6,14–22] Mutations in SOD1 decrease the stability of the dimeric species, causing dimer dissociation and unfolding.[22,23] Interestingly, the mutations having the largest effect on folding and thermodynamic stability are located on the surface of the protein, and not in the hydrophobic core.[24] Moreover, because intra-protein interactions are highly networked in SOD1, mutations of residues spread throughout the enzyme, and not only those near the dimer interface, might affect dissociation.[25] Other factors that destabilize the dimer interface

include the loss of metals and dissolution of the disulfide bond,[26] which are both promoted in SOD1 mutants. The resulting apo-monomer is the reactive species in protein aggregation of both wild type and mutant SOD1,[22,27,28] due to drastically reduced stability and partial unfolding.[26] However, the molecular details of progression along this aggregation pathway are still unclear.

Recently, Wilcox *et al*. reported post-translational modifications present in SOD1 purified from human erythrocytes.[29] The authors reported phosphorylation at Thr2 and glutathionylation at Cys111, both sites near the dimer interface. Wilcox *et al*. hypothesized that these post-translational modifications promote monomer formation, which leads to aggregation. They found a threefold increase in monomer formation for post-translationally modified species as compared to unmodified species when measured by size-exclusion chromatography. In an activity assay, modified species exhibited a twofold increase in K_d. This increase does not seem large, but such a change results in a 70% increase in the monomer population, which significantly increases the frequency of aggregation nucleation events.[29] Post-translational modifications present a possible link between familial and sporadic ALS, because they are present ubiquitously in varying amounts in the human population.[29–31] However, the molecular mechanism of dimer destabilization by post-translational modifications, glutathionylation in particular, is not yet understood.

The large size of glutathione and the location of both modifications at the dimer interface suggest a steric explanation of the dimer destabilization observed by Wilcox *et al*. We used all-atom discrete molecular dynamics simulations of modified and unmodified forms of the wild type and mutant monomer and dimer species to gain structural insight into the causes of increased dimer dissociation.[32] We used the replica exchange method to increase the sampling efficiency of our simulations for thermodynamic calculations.[33] We found that the processes of dimer dissociation and monomer unfolding are highly coupled, and that modification reduces but does not eliminate the coupled nature of the reaction. We discovered an unfolding intermediate structure common to wild type and mutant unmodified SOD1 dimer that precedes dimer dissociation in the unfolding pathway. Post-translational modification shifts the intermediate state to a lower energy, and decreases the potential energy gap (ΔE) between the native-like and dissociated states. In order to identify structural differences between modified and unmodified forms of SOD1 species, we used constant temperature simulations to avoid low- and high-temperature structural aberrations. We found differences in dimer interface contacts as a result of post-translational modification, which could explain the increased dimer dissociation of the post-translationally modified species.

Results

Thermodynamics of the dimer dissociation and monomer unfolding transition

On the basis of replica exchange simulations, we analyzed folding thermodynamics using the weighted histogram analysis method (WHAM), which incorporates multiple simulation trajectories with overlapping energetic sampling.[34] The density of states was calculated self-consistently by combining histograms from these multiple trajectories, and thereby thermodynamic parameters such as specific heat can be computed. Because we did not observe multiple unfolding and refolding transitions in our simulations due to insufficient sampling, we did not expect to obtain a fully quantitative free energy landscape for the various species of SOD1. However, we expected to gain insight into the stability of both the monomer and dimer species by using the unfolding transition temperature, which corresponds to the major peak in specific heat (Fig. 1; Supplementary Data Fig. 1).[26] Specific heat is a measure of the amount of energy necessary to increase the temperature (kinetic energy) of the protein. Hence, the peak in specific heat corresponds to a transition between energetic states, where energy is devoted to raising the potential as opposed to the kinetic energy of the complex. Monomer species exhibit one significant thermodynamic transition, corresponding to monomer unfolding (Fig. 1; Supplementary Data Fig. 1). Dimer species also exhibit one major transition, with the transition temperature shifted significantly to higher temperature as compared to the corresponding monomer species. Because the SOD1 dimer species feature one major peak rather than two peaks, corresponding to dimer dissociation and monomer unfolding, we conclude that dimer dissociation and monomer unfolding are highly coupled processes. The strong interactions in the dimer interface stabilize the individual monomers by shifting the unfolding transition to a higher temperature, keeping the dimer associated and folded at temperatures higher than the monomer unfolding temperature.

We observe that, in wild type and all mutant variants except A4V and I112T, modification causes a decrease in the coupled nature of the dissociation/unfolding transition. All unmodified species exhibit a single peak in specific heat, representing a single transition, but modified species feature a shoulder, representing a partial decoupling of the two processes (Fig. 1; Supplementary Data Fig. 1).

We find that modifications destabilize the dimer by shifting the transition temperature to a lower temperature. However, the effect of specific modification types on the dimer transition temperature varies between mutants (Supplementary Table 1).

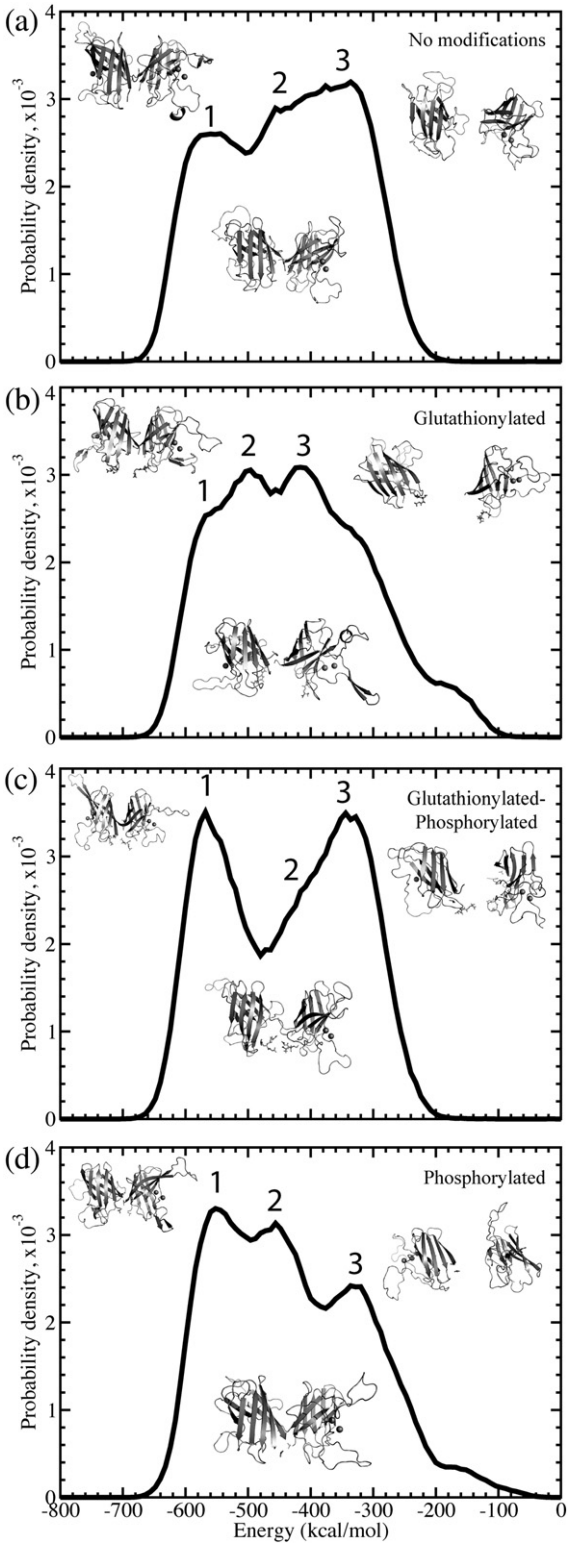

The exceptions to the destabilization trend are A4V, where the glutathionylated-phosphorylated dimer is stabilized in comparison with the unmodified dimer, and G93A, where all modified species are stabilized with respect to the unmodified form (Fig. 1; Supplementary Data Fig. 1).

We observe in dimer species that the maximum value of the major specific heat peak (corresponding to the energy input needed to raise the temperature of the complex by 1 °C during the dimer dissociation/unfolding transition) is highest in the unmodified species, as opposed to in the various modified species (Fig. 1; Supplementary Data Fig. 1), with the exceptions of G93A and I112T. The absolute value of the specific heat indicates the cooperativity of the phase transition. Therefore, this observation suggests that the dissociation/unfolding transitions are more cooperative in the unmodified species, and that modified species exhibit a more gradual melting transition from associated to dissociated states.

In monomer species, the unmodified form often exhibits the lowest specific heat peak for monomer unfolding (Fig. 1; Supplementary Data Fig. 1), which implies interactions between the modification molecules and the monomer, although these interactions do not affect the stability of the monomer. We expected this effect to some extent because the modified system is slightly larger. In agreement with recent experimental studies (R. L. Redler *et al.*, unpublished results), we found that modification did not have a large effect on monomer stability, although we observed a slight destabilization of the A4V monomer (Fig. 1; Supplementary Data Fig. 1 and Table S1).

Energetic states near the dissociation/unfolding transition

In order to study the more subtle transitions between native-like states that might explain an increased dissociation in modified species, it is necessary to examine the potential energy distributions of structures in the mid-range temperature region of the replica exchange simulations, 275–325 K, just reaching the lower bound of the dissociation/unfolding transition (Fig. 2; Supplementary Data Figs 2–6).These structures should include populations of native-like, dissociated and any intermediate states. All energies discussed are potential

Fig. 2. Deciphering the states for wild type. Distributions of total potential energies are shown with an unbroken curve. Potential energy is sampled throughout the simulations, at temperatures of 0.55–0.65 kcal (mol k_B)$^{-1}$, for (a) unmodified, (b) glutathionylated, (c) glutathionylated-phosphorylated and (d) phosphorylated cases of SOD1. The three Gaussian-like curves are highlighted for each species. Representative structures for each of the three states in each species are shown to the right of each plot.

energies of the system. In each system, we observed the existence of at least three low-energy states with Gaussian-like peaks or shoulders in the energy distribution. Because of the large size and close spacing of the surrounding populations, the distributions of some states as plotted on the energy coordinate (e.g. the second state in Fig. 2c) appear as shoulders. However, deconvolution of the peaks based on potential energies and subsequent clustering of structures within the energy window of each peak allows for the clear separation of these structural states. These low-energy states correspond to the native state and the early excitation states in the dissociation/unfolding process. Because the goal of this study was to uncover the effect of post-translational modifications on the dissociation process, we focus on these first three states by fitting each distribution to a trimodal Gaussian function and identifying the three lowest energy states present for each species. The first state is a low-energy state with a native-like structure; the second state has undergone a conformational change that can be characterized as a loosening of the β-barrels and/or a slight movement outwards of the two centers of mass (Figs. 3 and 4; Supplementary Data Figures 7–11 and Table S2); and the third state is the dissociated state, with partial unfolding due to the coupled nature of the dissociation and unfolding processes.

The amount of differentiation between the states in partial unfolding or separation of the monomers varies with mutant and modification type. Although in some glutathionylated species, namely A4V-GSH, G37R-GSH, G93A-GSH-P_i, H46R-GSH-P_i and I112T-GSH, the representative structure of the intermediate energetic state is dissociated (Supplementary Data Figs 2–6), we observe from the distributions of monomer separation and monomer unfolding that, statistically, the intermediate state as a whole is still distinct from the dissociated state (Supplementary Data Figs 7–11). In G93A, the unmodified species exhibit an intermediate state that maintains very few dimer interface contacts and, therefore, has a larger tendency to be dissociated than the intermediate states of other mutant variants. However, modification restores the intermediate state to a form with similar characteristics to the other mutants. We observed also that in the phosphorylated species of G37R, G37R-GSH-P_i and G37R-P_i, phosphorylation causes the third state to have a larger population of associated structures than is seen in other species. However, as discussed above, the second and third states are still distinct when characterized by their distributions of monomer separation and unfolding among all structures (Supplementary Data Fig. 8).

In general, we found that modification increased dissociation by decreasing the potential energy gap between the native-like and the dissociated states, as opposed to only destabilizing the native-like state. In most mutant variants, the native-like state, which occurs at approximately –550 kcal mol^{-1} but varying across mutant variants, does not undergo a significant energetic change upon modification (Fig. 2; Supplementary Data Figs 2–6 and Table S3). However, the intermediate state population is shifted to a lower energy in modified species, with exceptions in some phosphorylated species: wild type-GSH-P_i, G37R-P_i, H46R-GSH-P_i, and I112T-P_i. Stabilization of this dissociation/unfolding intermediate increases the probability of the protein to misfold and dissociate. In many of the modified species, the third (dissociated) state is also stabilized as compared to the third state in the unmodified species, with exceptions in wild type phosphorylated species, all A4V modified species, G93A-GSH-P_i and I112T-GSH. In general, we find that the overall ΔE between the native-like and the dissociated populations is decreased in modified cases as compared to unmodified, with the exceptions of wild type-GSH-P_i, all modified species of A4V, G93A-GSH-P_i and I112T-GSH (Fig. 2, Supplementary Data Figs 2–6 and Table S3).

Structural changes induced by post-translational modifications

Modification affects the interactions between the two monomers and causes structural rearrangement. The two monomers of SOD1 can be represented as cylinders that, instead of being oriented in a parallel fashion, are positioned at a torsional angle to one another (Fig. 4a). In constant temperature simulations, we note that this torsional angle is affected by modification, which occurs near the dimer interface, but the effect is different for different mutants (Fig. 4; Supplementary Data Fig. 12). These differences are potentially due to variation between the mutants in their dimer interface configuration and how they are affected by the addition of the modification molecule (Supplementary Data Figs 13–18).

We observe a major difference in dimer interface interactions between wild type and the various mutant SOD1s in constant temperature simulations. Where wild type exhibits monomer–monomer interactions between residues located throughout the length of the protein sequence, mutant SOD1 monomer–monomer interactions almost exclusively involve a terminus from at least one of the monomers, with the exception of the structurally wild type-like G93A. This property is manifested in the interface contact maps of each species (Supplementary Data Figs 13–18): wild type has significant interactions present in the center of the map, whereas the center of the map for the various mutant SOD1s is blank. It might be for this reason that modifications introduce an asymmetry in

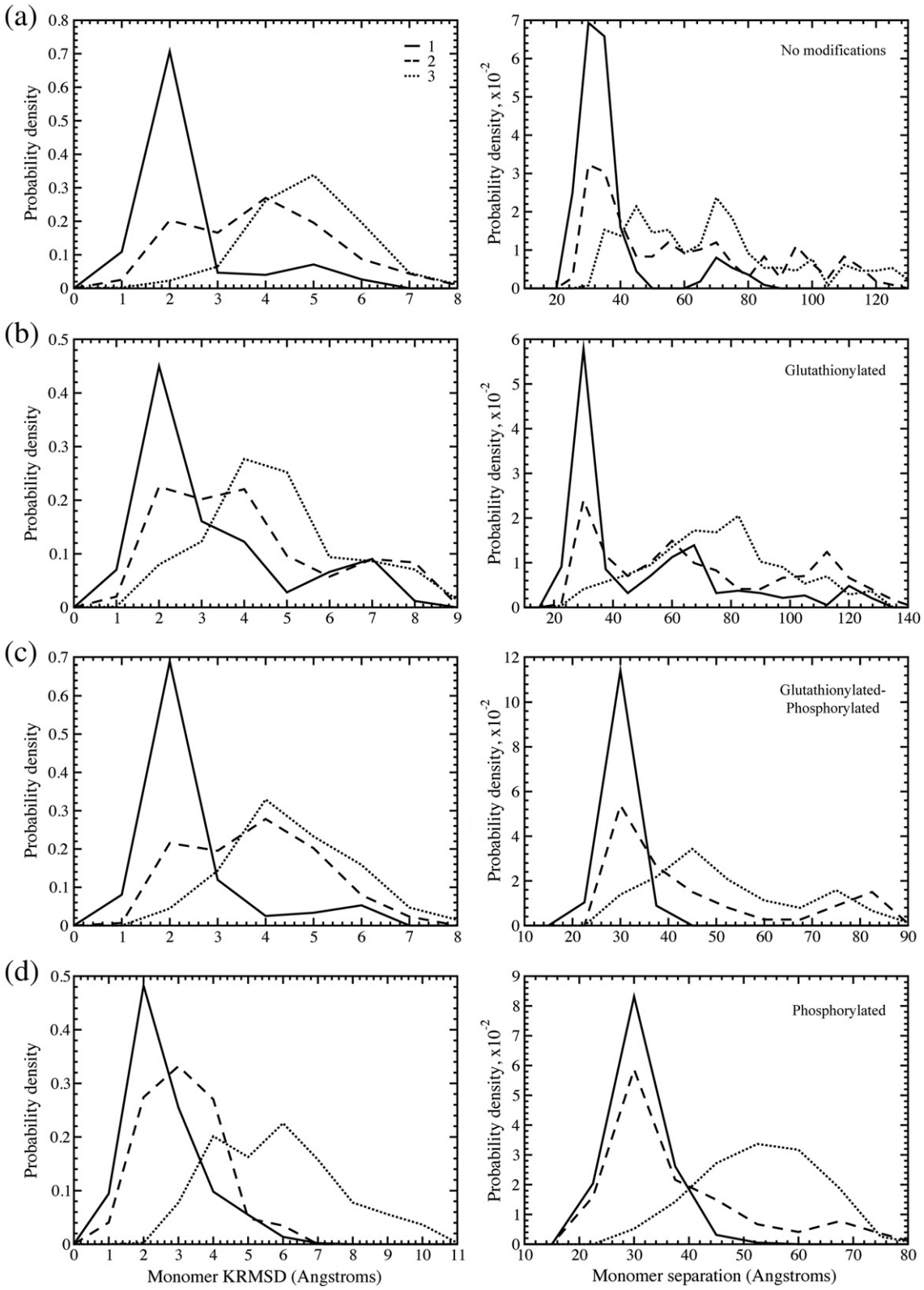

Fig. 3 (*legend on next page*)

monomer–monomer interactions in only the wild type enzyme. For instance, in wild type–GSH we observe that interactions near 60A–115B (A and B represent the two monomers) have disappeared when compared to the unmodified, but 115A–60B interactions remain (Supplementary Data Fig. 13B). Also, in some residues one monomer might see only a shift in interface contacts, losing interaction frequency in one residue but gaining it in an adjacent residue, while the other monomer loses contacts with no compensating gain. This compromise could introduce strain into the structure that leads to the increased dissociation seen experimentally (R. L., Redler *et al*. unpublished results).[29]

In contrast to the wild type, mutant SOD1 is affected symmetrically in the two monomers by modification. In A4V, we find a loss of interactions in the dimer interface of the glutathionylated species, and in the phosphorylated species we observe increased interface contacts near the C termini and decreased or shifting interactions elsewhere (Supplementary Data Fig. 14). In the G37R mutant, we find a shifting of contacts in the C termini, implying a structural movement in that area (Supplementary Data Fig. 15). In G93A, we observe an overall increase in interface contacts upon modification, implying that the introduction of the modification molecules induces the formation of non-native interactions in the interface (Supplementary Data Fig. 16). upon modification, H46R loses contacts in all areas of the interface, although in the phosphorylated species the interactions in the N and C termini are shifted rather than lost (Supplementary Data Fig. 17), which can be seen in added contacts directly adjacent to the lost contacts. In I112T, most losses of contacts are accompanied by a gain in the residues directly adjacent (Supplementary Data Fig. 18), which would imply a shift in the location of the dimer interface and, therefore, a shift in its make-up.

Cumulatively, these results imply a shift in the composition and position of the dimer interface upon modification. A change in the identity, even if not the number, of dimer interface contacts could result in the loss of monomer–monomer binding affinity and increased dimer dissociation. In a parallel experimental study, Redler *et al.* found a shift towards the monomer population in wild type and mutant A4V SOD1, and an increase in the rate of monomer formation in mutant I112T SOD1 (R. L. Redler *et al*. unpublished results), which would suggest that the contact loss seen in wild type-GSH and A4V-GSH (Supplementary Data Figs 13 and 14) results in a loss of monomer–monomer binding affinity, whereas the overall shift in contacts seen in I112T-GSH (Supplementary Data Fig. 14) results in an increased k_{off} for the dissociation reaction (R. L. Redler *et al*. unpublished results).

Predictably, we observe in constant temperature simulations that the modification molecules interact most frequently with the residues surrounding the modification site on their associated monomer (Supplementary Data Figs 19 and 20). In fact, the modification molecules interact almost exclusively with their associated monomer. Interactions with the opposing monomer or with the opposing modification molecule are comparatively infrequent and do not occur in all mutant variants. The locations of the interacting residues in small loop segments connecting the β-strands (Fig. 5) could pull apart the β-barrels, which would result in the loss of crucial contacts and therefore dissociation.

Discussion

Our systematic replica exchange DMD simulations indicate a strong coupling of the dimer dissociation and monomer unfolding processes, which has important implications for overall protein stability and aggregation. Dimerization significantly stabilizes the folded monomer, which implies that contacts in the dimer interface contribute to the integrity of the monomer β-barrels. As these contacts are broken, the intra-monomer interactions maintaining the β-barrel formation of each monomer are also broken, causing simultaneous dissociation and partial unfolding. The unfolding process is then more favorable to complete upon full dissociation.

Similarly, the wild type and mutant unmodified species in general dissociate and unfold more sharply than the modified forms with an increase in temperature (Fig. 1; Supplementary Data Fig. 1). This finding implies that the shifting or gain of non-native contacts (Supplementary Data Figs 13–18) that occurs in modified species causes a loss of cooperativity in the interface and intra-monomer interactions. This loss of cooperativity allows some contacts to be lost much more frequently than others, whether due to a structural change or the steric interference of the modification molecules. A loss in interaction cooperativity might be manifest in the stabilization of the intermediate state and this

Fig. 3. Structural characterization of energetic populations in wild type SOD1. Distributions of values for the monomer aligned KRMSD from the starting structure, used as a measure of β-barrel integrity and unfolding (left column), and the distance between monomer centers of mass, used as a measure of dissociation (right column). We show distributions for (a) unmodified, (b) glutathionylated, (c) glutathionylated-phosphorylated and (D) phosphorylated wild type SOD1 for the first, second and third energy populations described for Fig. 2. The legend shown for (a) is relevant for all panels.

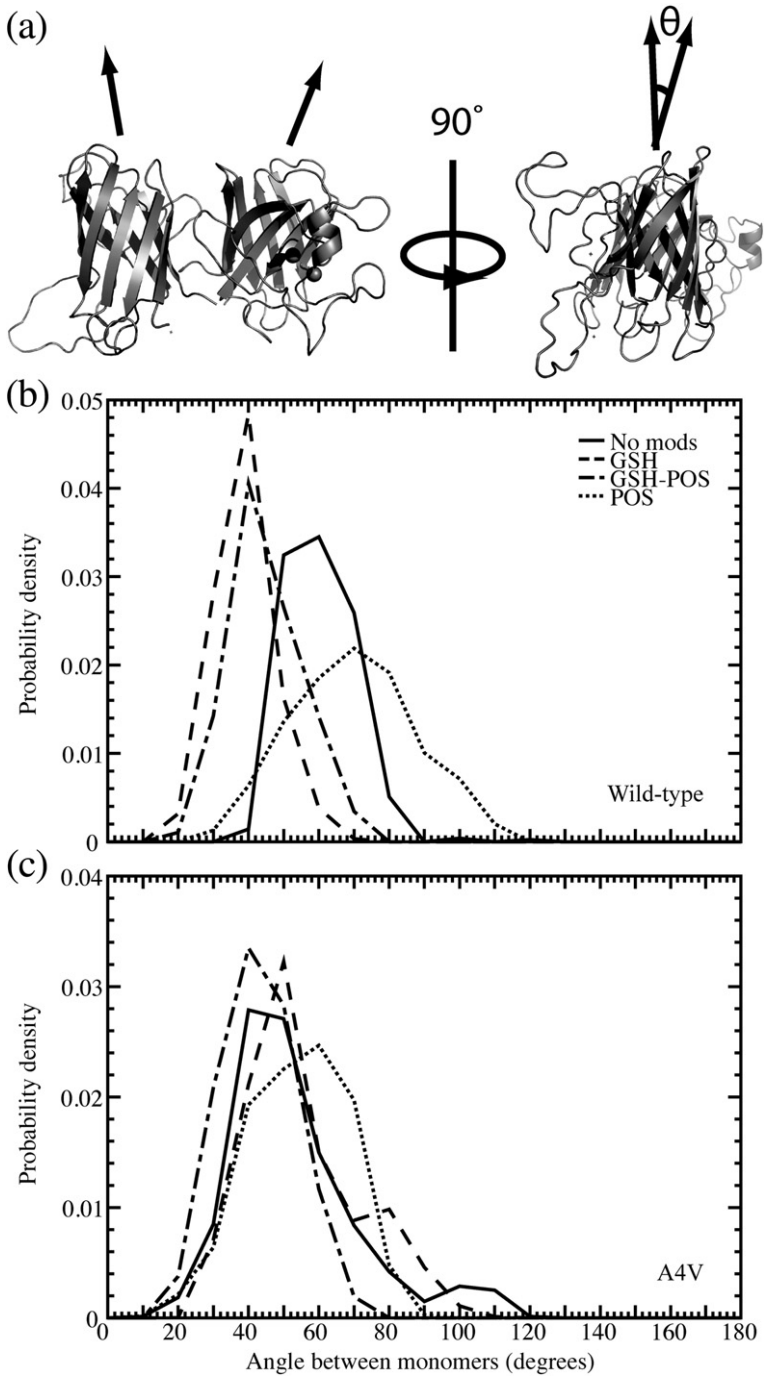

Fig. 4. Structural effects of modification on the angle between monomers in the SOD1 dimer. (a) Depiction of the angle, θ, measured between monomers in the SOD1 dimer. Distribution of angle between monomers in constant temperature populations of modified and unmodified (b) wild type and (c) A4V dimer. The legend shown for (b) is relevant also for (c).

could be the reason for the decreased potential energy gap between the native and dissociated states (Fig. 2, Supplementary Data Figs 2–6 and Table S3). Interactions between the modifications and their associated monomer might also be responsible for this more drawn out dissociation interaction and loss of cooperativity; both modifications are located near the dimer interface (Fig. 5), and their interactions with the monomers could disrupt or weaken native interface interactions. This effect could possibly be remedied by the introduction of additional interactions in the form of a drug that would bind, bridging the dimer interface and holding it together, as was found by Ray *et al.*[35] In

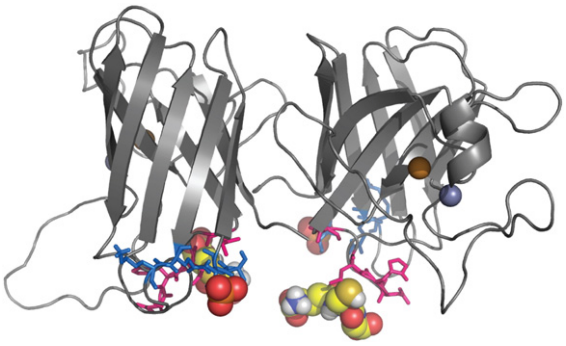

Fig. 5. Residues interacting with modifications. Residues having the highest frequency of interaction with phosphate are shown in marine blue, and those with glutathione are shown in hot pink. Modification molecules are shown as spheres.

addition, it might be possible to design a drug that would interfere with the modification of SOD1 in the first place, whether by occupation or blocking of the modification site or inhibition of the modification binding itself.

The results discussed above indicate that the post-translational modifications glutathionylation and phosphorylation affect the energetic and structural properties of wild type and mutant SOD1. The effect observed varies with both mutant and modification. This observation suggests that different types of modification have varied effects on the stability of the dimer of the various genetic mutations, and for different reasons. For example, the A4V dimer appears to be largely stabilized by modification, while the wild type dimer is destabilized by glutathionylation but appears to be "rescued" from this effect by phosphorylation. Glutathionylation in particular, with the exceptions of A4V and I112T, has a dramatic effect on decreasing the potential energy gap between the native-like state and the dissociated state. We infer from this that the presence of glutathione, a marker of oxidative stress in the cell,[36] would be detrimental in most types of familial ALS. This finding corroborates with reports that exercise[37] and electrical stimulation[38] of ALS model animals results in a more rapid and severe disease progression, because both of these would produce increased oxidative stress in cells and hence increased levels of glutathionylated protein.[39] An environmental factor such as oxidative stress could help to explain the differences in disease progression between the various ALS-causative mutants.

Our simulation results indicate that post-translational modifications in wild type and mutant A4V SOD1 result in a net loss in the total number of interface contacts and, thus, a reduced binding energy. This result is consistent with the experimental observation of reduced dimer dissociation constant in modified wild type and A4V mutant (R. L. Redler *et al.*, unpublished results). Our simulations of the I112T mutant suggest that the modification induces a shift in the dimer interface, but no significant change in the total number of contacts, in contrast to the wild type and the A4V mutant. This result suggests that modified I112T has a dimer dissociation constant similar to that of the unmodified species. Indeed, Redler *et al.* showed that the equilibrium constant of I112T dimer dissociation is not affected by glutathionylation.

Here, we studied homo-modified species of wild type and mutant SOD1. However, it is possible that *in vivo* SOD1 might exhibit significant hetero-modified populations in addition to homo-modified species. Because of the means of experimental characterization of post-translational modifications from erythrocytes (mass spectrometry; R. L. Redler et al., unpublished results),[29] dimers are necessarily dissociated before measurement, and so it is impossible to determine whether dimers are hetero- or homo-modified *in vivo* using this method. The molecular mechanism of glutathionylation, as well as the kinase responsible for phosphorylation of SOD1, are still unknown, so it is unclear whether modification of the individual monomers is a cooperative or an independent process. However, even the presence of only one modified molecule near the dimer interface disrupts or changes monomer–monomer contacts and induces many of the same effects that we observe in homo-modified species.

On a further note, because glutathionylation decreases the potential energy gap between the native-like and dissociated states in wild type SOD1, and glutathionylation of SOD1 is present even in healthy individuals,[29] it is possible that glutathionylation caused by oxidative stress to motor neurons could be a factor in sporadic ALS. The late onset of ALS suggests that an environmental trigger could exist for both familial and sporadic cases. This possibility fits with the increased occurrence of sporadic ALS in athletes[40] and soldiers[41] as compared to the general population; both of these groups experience more extreme and frequent oxidative stress than does the average individual. Such environmental factors could possibly be counteracted with a drug or lifestyle decisions. Further investigation into the mechanism of post-translational modification in SOD1 could illuminate preventative measures against the observed increased dissociation and unfolding, and hence inhibit aggregation and disease.

Materials and Methods

All-atom discrete molecular dynamics (DMD)

A complete description of the DMD algorithm can be found elsewhere.[42,43] Briefly, DMD utilizes discrete step

function potentials to govern inter-atomic interactions, as opposed to the continuous potentials used in traditional molecular dynamics (MD). The velocity of each atom is constant until a collision occurs at the step of the potential function, at which point the velocity of the atom changes instantaneously according to the laws of conservation of energy, momentum and angular momentum. A collision table records all possible collisions between neighboring atoms, and the next collision is obtained by sorting these possible collisions. At each collision, only the colliding atoms have their positions and velocities updated, and the corresponding possible collisions of these two atoms are updated in the collision table. As a result, this innovation allows for a significant decrease in the number of calculations needed per simulation time step. Having fewer and faster calculations allows DMD to achieve a significant increase in sampling over MD.

In the all-atom protein model for DMD,[32] all heavy atoms and polar hydrogen atoms are explicitly represented. We represent bonded interactions by placing infinite square-well constraints on bond lengths, bond angles and dihedral angles. Non-bonded interactions are adapted from the Medusa force field.[44] The van der Waals interactions are modeled using the standard Lennard–Jones potential, while solvation interactions are modeled by the Lazaridis–Karplus solvation model.[45] Both potentials are discretized by multi-step square-well functions, characterized by the hard-core atom radius and a series of potential steps. We model hydrogen bonding interactions by the reaction algorithm.[46]

Systems studied

We used constant volume DMD simulations with periodic boundary conditions for both monomer and dimer SOD1 and we studied the disease-relevant mutants A4V, G37R, G93A, H46R and I112T, as well as wild type SOD1. For each system of monomer or dimer and mutant or wild type, we studied modifications consisting of glutathionylated (GSH), glutathionylated-phosphorylated (GSH-P_i), and phosphorylated (P_i), as well as unmodified structures, resulting in a total of 48 systems (6 (five mutants and wild type) × 2 (monomer or dimer) × 4 (modification types)). For simplicity, we refer to each mutation–modification combination (e.g. A4V-GSH-P_i, G93A-unmodified, wild type-P_i) as a species. For instance, dimer species refers to all mutation–modification combinations in their dimerized form. For each species, we performed both replica exchange and constant temperature DMD simulations.

Modeling of modified SOD

We obtained structures of post-translationally modified mutant and wild type SOD1 using the known X-ray crystallographic structure of wild type SOD1 (PDBID 1SPD) as a reference structure. We constrained glutathione and/or phosphate molecules to their respective SOD1 residues (Thr2 for phosphate and Cys111 for glutathione). We obtained parameters for bond length, angle and dihedral constraints for glutathione, metals, and disulfide bonds from the CHARMM19 force field.[45] All dimers were homo-modified. We then mutated the wild type structure to generate each disease-relevant mutant (A4V, G37R, G93A, H46R and I112T) using the Eris suite.[47,48] We made no structural adjustment to residues participating in metal-binding, glutathionylation, phosphorylation or disulfide bond interactions unless they are necessary to the system of interest, as in the case of H46R, which coordinates the catalytic copper ion.

In order to minimize steric clashing between modifications and the SOD1 protein and to relax the SOD1 backbone, we used an iterative relaxation and equilibration of each system utilizing all-atom DMD (as described above). We performed three simulation iterations, each with a progressively lower heat exchange rate (0.2, 0.02 and 0.002 fs^{-1}, respectively). Each iteration was performed for 50 ps at a reduced unit temperature of 0.5 kcal (mol $k_B)^{-1}$ (~251 K).

Replica exchange

We used the replica exchange method to perform simulations of multiple copies of the same system in parallel at various temperatures.[33] To fully explore protein conformational space, the upper end of the temperature range should be enough to unfold the protein. At given time intervals, replicas of neighboring temperatures exchange temperature values according to a Metropolis-based stochastic algorithm. We set the temperature exchange interval as 50 ps. Exchange between replicas increases sampling efficiency in that energetic barriers can be overcome more easily, and in less time, with exposure to higher temperatures.

In the monomer species, 12 replicas were used for a simulation length of 100 ns at temperatures of 0.50 (~252 K), 0.52 (~262 K), 0.54 (~272 K), 0.56 (~282 K), 0.58 (~292 K), 0.60 (~302 K), 0.62 (~312 K), 0.64 (~322 K), 0.66 (~332 K), 0.68 (~343 K), 0.70 (~353 K) and 0.72 (~363 K) kcal mol^{-1}. In the dimer species, 16 replicas were used for a simulation length of 50 ns at temperatures of 0.48 (~242 K), 0.495 (~249 K), 0.51 (~257 K), 0.525 (~264 K), 0.54 (~272 K), 0.555 (~280 K), 0.57 (~287 K), 0.585 (~295 K), 0.60 (~302 K), 0.615 (~310 K), 0.63 (~317 K), 0.645 (~325 K), 0.65 (~327 K), 0.67 (~337 K), 0.69 (~347 K) and 0.71 (~357 K) kcal (mol $k_B)^{-1}$. It is important to note that the temperatures used in MD simulations, including DMD simulations, often do not equate directly with physical temperatures. For example, the calculated melting temperature of wild type SOD1 dimer is different from the experimentally measured value of 93°C (366 K).[49] However, the simulations can be used to evaluate the relative changes in temperature, which are relevant to our studies.

Replica trajectories were combined for the analysis of folding thermodynamics using the weighted histogram analysis method (WHAM).[34] It is important to have sufficient sampling of the energetic sates in thermodynamics calculations. To test our sampling, we split our simulation trajectories in half and compared the distribution of energies for the two halves. We obtained similar results for both halves and concluded that sampling was sufficient to reach equilibrium.

WHAM analysis of C_V

We used the MMTSB tool[50] for WHAM analysis of the replica exchange simulations. WHAM computes the

density of states by combining histograms from overlapping simulation trajectories. Given the density of states $\rho(E)$, the folding specific heat at constant volume, C_V, is computed at various temperatures according to the partition function:

$$Z = \int dE \rho(E) exp(-E / kT)$$

where E is the potential energy.

Identification of states

We calculate specific heat according to temperature using WHAM.[34] We calculate potential energy distributions over each simulation using intermediate temperatures (275–325 K) so as not to introduce structural aberrations in representative structures from low- and high-temperature conditions. Contributions from internal potential energy of the modification molecules are minimal in comparison to the potential energy of the system; therefore, no adjustment is needed for comparisons of potential energy between modification systems. We fit each energy distribution with a trimodal Gaussian, corresponding to the three lowest energy peaks and/or shoulders in the distribution, and identify the energy of each state as the mean of its respective Gaussian function. Because the individual Gaussian functions corresponding to each state overlap significantly, and deconvolution with respect to individual structures is not possible, we identify representative structures by clustering structures whose energies fall within 1 kcal mol^{-1} around the mean of the respective Gaussian by RMSD using the OC suite‡. Structures with energies in this range have a higher probability of belonging to the energetic state of interest than of being a member of the tail of one of the other states. We choose RMSD cutoffs for clustering as the global maximum in a histogram of pairwise RMSDs of all structures clustered. We choose the centroid of the largest cluster as the representative structure for each state. The largest cluster is in all cases at least four times the weight of the next-largest cluster.

Measurement of angle between monomers

We define the radial axis vector for each monomer by creating vectors along each β-strand making up the approximately cylindrical β-barrel, and averaging over the components. We define all β-strand vectors to have the same directionality sign, and we length-normalize the vectors before averaging. The representative vector therefore has the three-dimensional average direction of all β-strand vectors in each monomer. In order for these calculations to be meaningful, structures must be both folded and associated. In order to eliminate structures with monomer unfolding, for each simulation snapshot (snapshots recorded every 5 ps) we calculate the aligned RMSD (Kabsch RMSD,[51] KRMSD) between the β-barrel alpha carbons of each monomer of the initial wild type-like structure (see Modeling of modified SOD1 above) and those of the corresponding monomer of the structural snapshot. We impose a KRMSD cutoff of 4 Å, which we choose on the basis of the distribution of KRMSD values from all snapshots of all simulated species. To eliminate dissociated structures, we measure the distance between the centers of mass of the two monomers, which are calculated on the basis of the alpha carbons in the β-barrels. We impose a cutoff of 35 Å, which we choose in the same manner as the cutoff for KRMSD. We retain those structures of each species that meet the criteria for both folded and associated, and measure the angle between the vectors characterizing the two monomers. The angle between the two vectors v_1 and v_2 is calculated as:

$$\theta = \arccos\left(\frac{\vec{v_1} \cdot \vec{v_2}}{||a||\,||b||}\right)$$

Interface contact maps

We define two residues as being in contact in the dimer interface if the two alpha carbons are within 10 Å of each other. At each simulation snapshot, we evaluate contacts between the two monomeric chains. The count between every pair of residues is normalized for the total number of simulation snapshots.

Modification hit maps

We define a molecule as being in contact with a residue or another molecule if any heavy atom in the molecule is within 4.5 Å of any heavy atom in the residue or second molecule. Contact counts are recorded and normalized essentially as described above for the interface contact maps.

‡ Barton, G.J. (1993, 2002) OC - A cluster analysis program, University of Dundee, Scotland, UK; www.compbio.dundee.ac.uk/downloads/oc

Acknowledgements

The authors thank Dr Michael Caplow, Rachel Redler, Dr Kyle Wilcox, Dr Lanette Fee, Pradeep Kota and Srinivas Ramachandran for helpful discussions. This work was supported by the National Institutes of Health grant number R01GM080742 and ARRA supplements GM080742-03S1 and GM066940-06S1. E.A.P. was supported by the UNC Curriculum in Bioinformatics and Computational Biology and National Institute of Health Predoctoral Fellowship F31AG039266-01 from the National Institute on Aging.

Supplementary Data

Supplementary materials related to this article can be found online at doi:10.1016/j.jmb.2011.03.004

References

1. Cleveland, D. W. & Rothstein, J. D. (2001). From Charcot to Lou Gehrig: deciphering selective motor neuron death in ALS. *Nat. Rev. Neurosci.* **2**, 806–819.
2. Rosen, D. R. (1993). Mutations in Cu/Zn superoxide dismutase gene are associated with familial amyotrophic lateral sclerosis. *Nature*, **364**, 362.
3. Getzoff, E. D., Tainer, J. A., Stempien, M. M., Bell, G. I. & Hallewell, R. A. (1989). Evolution of CuZn superoxide dismutase and the Greek key beta-barrel structural motif. *Proteins*, **5**, 322–336.
4. Perry, J. J., Shin, D. S., Getzoff, E. D. & Tainer, J. A. (2010). The structural biochemistry of the superoxide dismutases. *Biochim. Biophys. Acta*, **1804**, 245–262.
5. Kayatekin, C., Zitzewitz, J. A. & Matthews, C. R. (2008). Zinc binding modulates the entire folding free energy surface of human Cu,Zn superoxide dismutase. *J. Mol. Biol.* **384**, 540–555.
6. Rumfeldt, J. A., Lepock, J. R. & Meiering, E. M. (2009). Unfolding and folding kinetics of amyotrophic lateral sclerosis-associated mutant Cu,Zn superoxide dismutases. *J. Mol. Biol.* **385**, 278–298.
7. Tainer, J. A., Getzoff, E. D., Beem, K. M., Richardson, J. S. & Richardson, D. C. (1982). Determination and analysis of the 2 Å-structure of copper, zinc superoxide dismutase. *J. Mol. Biol.* **160**, 181–217.
8. Lindberg, M. J., Normark, J., Holmgren, A. & Oliveberg, M. (2004). Folding of human superoxide dismutase: disulfide reduction prevents dimerization and produces marginally stable monomers. *Proc. Natl Acad. Sci. USA*, **101**, 15893–15898.
9. Hornberg, A., Logan, D. T., Marklund, S. L. & Oliveberg, M. (2007). The coupling between disulphide status, metallation and dimer interface strength in Cu/Zn superoxide dismutase. *J. Mol. Biol.* **365**, 333–342.
10. McCord, J. M. & Fridovich, I. (1969). Superoxide dismutase. An enzymic function for erythrocuprein (hemocuprein). *J. Biol. Chem.* **244**, 6049–6055.
11. Valentine, J. S. & Hart, P. J. (2003). Misfolded CuZnSOD and amyotrophic lateral sclerosis. *Proc. Natl Acad. Sci. USA*, **100**, 3617–3622.
12. Chou, S. M., Wang, H. S. & Komai, K. (1996). Colocalization of NOS and SOD1 in neurofilament accumulation within motor neurons of amyotrophic lateral sclerosis: an immunohistochemical study. *J. Chem. Neuroanat.* **10**, 249–258.
13. Chou, S. M., Wang, H. S. & Taniguchi, A. (1996). Role of SOD-1 and nitric oxide/cyclic GMP cascade on neurofilament aggregation in ALS/MND. *J. Neurol. Sci.* **139**, 16–26.
14. Lindberg, M. J., Tibell, L. & Oliveberg, M. (2002). Common denominator of Cu/Zn superoxide dismutase mutants associated with amyotrophic lateral sclerosis: decreased stability of the apo state. *Proc. Natl Acad. Sci. USA*, **99**, 16607–16612.
15. Stathopulos, P. B., Rumfeldt, J. A., Scholz, G. A., Irani, R. A., Frey, H. E., Hallewell, R. A. *et al.* (2003). Cu/Zn superoxide dismutase mutants associated with amyotrophic lateral sclerosis show enhanced formation of aggregates in vitro. *Proc. Natl Acad. Sci. USA*, **100**, 7021–7026.
16. Lindberg, M. J., Bystrom, R., Boknas, N., Andersen, P. M. & Oliveberg, M. (2005). Systematically perturbed folding patterns of amyotrophic lateral sclerosis (ALS)-associated SOD1 mutants. *Proc. Natl Acad. Sci. USA*, **102**, 9754–9759.
17. Svensson, A. K., Bilsel, O., Kondrashkina, E., Zitzewitz, J. A. & Matthews, C. R. (2006). Mapping the folding free energy surface for metal-free human Cu,Zn superoxide dismutase. *J. Mol. Biol.* **364**, 1084–1102.
18. Vassall, K. A., Stathopulos, P. B., Rumfeldt, J. A., Lepock, J. R. & Meiering, E. M. (2006). Equilibrium thermodynamic analysis of amyotrophic lateral sclerosis-associated mutant apo Cu,Zn superoxide dismutases. *Biochemistry*, **45**, 7366–7379.
19. Rumfeldt, J. A., Stathopulos, P. B., Chakrabarrty, A., Lepock, J. R. & Meiering, E. M. (2006). Mechanism and thermodynamics of guanidinium chloride-induced denaturation of ALS-associated mutant Cu,Zn superoxide dismutases. *J. Mol. Biol.* **355**, 106–123.
20. Mulligan, V. K., Kerman, A., Ho, S. & Chakrabartty, A. (2008). Denaturational stress induces formation of zinc-deficient monomers of Cu,Zn superoxide dismutase: implications for pathogenesis in amyotrophic lateral sclerosis. *J. Mol. Biol.* **383**, 424–436.
21. Nordlund, A., Leinartaite, L., Saraboji, K., Aisenbrey, C., Grobner, G., Zetterstrom, P. *et al.* (2009). Functional features cause misfolding of the ALS-provoking enzyme SOD1. *Proc. Natl Acad. Sci. USA,*, **106**, 9667–9672.
22. Khare, S. D., Caplow, M. & Dokholyan, N. V. (2006). FALS mutations in Cu,Zn superoxide dismutase destabilize the dimer and increase dimer dissociation propensity: a large-scale thermodynamic analysis. *Amyloid*, **13**, 226–235.
23. Rodriguez, J. A., Shaw, B. F., Durazo, A., Sohn, S. H., Doucette, P. A., Nersissian, A. M. *et al.* (2005). Destabilization of apoprotein is insufficient to explain Cu,Zn-superoxide dismutase-linked ALS pathogenesis. *Proc. Natl Acad. Sci. USA*, **102**, 10516–10521.
24. Khare, S. D., Ding, F. & Dokholyan, N. V. (2003). Folding of Cu,Zn superoxide dismutase and familial amyotrophic lateral sclerosis. *J. Mol. Biol.* **334**, 515–525.
25. Khare, S. D. & Dokholyan, N. V. (2006). Common dynamical signatures of familial amyotrophic lateral sclerosis-associated structurally diverse Cu,Zn superoxide dismutase mutants. *Proc. Natl Acad. Sci. USA*, **103**, 3147–3152.
26. Ding, F. & Dokholyan, N. V. (2008). Dynamical roles of metal ions and the disulfide bond in Cu,Zn superoxide dismutase folding and aggregation. *Proc. Natl Acad. Sci. USA*, **105**, 19696–19701.
27. Rakhit, R., Crow, J. P., Lepock, J. R., Kondejewski, L. H., Cashman, N. R. & Chakrabartty, A. (2004). Monomeric Cu,Zn-superoxide dismutase is a common misfolding intermediate in the oxidation models of sporadic and familial amyotrophic lateral sclerosis. *J. Biol. Chem.* **279**, 15499–15504.
28. Chattopadhyay, M., Durazo, A., Sohn, S. H., Strong, C. D., Gralla, E. B., Whitelegge, J. P. & Valentine, J. S. (2008). Initiation and elongation in fibrillation of ALS-linked superoxide dismutase. *Proc. Natl Acad. Sci. USA*, **105**, 18663–18668.
29. Wilcox, K. C., Zhou, L., Jordon, J. K., Huang, Y., Yu, Y., Redler, R. L. *et al.* (2009). Modifications of superoxide dismutase (SOD1) in human erythrocytes: a possible role in amyotrophic lateral sclerosis. *J. Biol. Chem.* **284**, 13940–13947.

30. Nakanishi, T., Kishikawa, M., Miyazaki, A., Shimizu, A., Ogawa, Y., Sakoda, S. *et al.* (1998). Simple and defined method to detect the SOD-1 mutants from patients with familial amyotrophic lateral sclerosis by mass spectrometry. *J. Neurosci. Methods*, **81**, 41–44.
31. Marklund, S. L., Andersen, P. M., Forsgren, L., Nilsson, P., Ohlsson, P. I., Wikander, G. & Oberg, A. (1997). Normal binding and reactivity of copper in mutant superoxide dismutase isolated from amyotrophic lateral sclerosis patients. *J. Neurochem.* **69**, 675–681.
32. Ding, F., Tsao, D., Nie, H. & Dokholyan, N. V. (2008). Ab initio folding of proteins with all-atom discrete molecular dynamics. *Structure*, **16**, 1010–1018.
33. Okamoto, Y. (2004). Generalized-ensemble algorithms: enhanced sampling techniques for Monte Carlo and molecular dynamics simulations. *J. Mol. Graph. Model*, **22**, 425–439.
34. Kumar, S., Rosenberg, J. M., Bouzida, D., Swendsen, R. H. & Kollman, P. (1992). THE weighted histogram analysis method for free-energy calculations on biomolecules. I. The method. *J. Comput. Chem.* **13**, 1011–1021.
35. Ray, S. S., Nowak, R. J., Brown, R. H., Jr & Lansbury, P. T., Jr (2005). Small-molecule-mediated stabilization of familial amyotrophic lateral sclerosis-linked superoxide dismutase mutants against unfolding and aggregation. *Proc. Natl Acad. Sci. USA*, **102**, 3639–3644.
36. Townsend, D. M. (2007). *S*-Glutathionylation: indicator of cell stress and regulator of the unfolded protein response. *Mol. Interv.* **7**, 313–324.
37. Chen, A., Montes, J. & Mitsumoto, H. (2008). The role of exercise in amyotrophic lateral sclerosis. *Phys. Med. Rehabil. Clin. N. Am.* **19**, 545–557.
38. Lepore, A. C., Tolmie, C., O'Donnell, J., Wright, M. C., Dejea, C., Rauck, B. *et al.* (2010). Peripheral hyperstimulation alters site of disease onset and course in SOD1 rats. *Neurobiol. Dis.* **39**, 252–264.
39. Powers, S. K. & Jackson, M. J. (2008). Exercise-induced oxidative stress: cellular mechanisms and impact on muscle force production. *Physiol. Rev.* **88**, 1243–1276.
40. Chio, A., Traynor, B. J., Swingler, R., Mitchell, D., Hardiman, O., Mora, G. *et al.* (2008). Amyotrophic lateral sclerosis and soccer: a different epidemiological approach strengthen the previous findings. *J. Neurol. Sci.* **269**, 187–189.
41. Horner, R. D., Kamins, K. G., Feussner, J. R., Grambow, S. C., Hoff-Lindquist, J., Harati, Y. *et al.* (2003). Occurrence of amyotrophic lateral sclerosis among Gulf War veterans. *Neurology*, **61**, 742–749.
42. Dokholyan, N. V., Buldyrev, S. V., Stanley, H. E. & Shakhnovich, E. I. (1998). Discrete molecular dynamics studies of the folding of a protein-like model. *Fold. Des.* **3**, 577–587.
43. Zhou, Y. & Karplus, M. (1997). Folding thermodynamics of a model three-helix-bundle protein. *Proc. Natl Acad. Sci. USA*, **94**, 14429–14432.
44. Ding, F. & Dokholyan, N. V. (2006). Emergence of protein fold families through rational design. *PLoS Comput. Biol.* **e85**, 2.
45. Lazaridis, T. & Karplus, M. (1999). Effective energy function for proteins in solution. *Proteins*, **35**, 133–152.
46. Ding, F., Borreguero, J. M., Buldyrey, S. V., Stanley, H. E. & Dokholyan, N. V. (2003). Mechanism for the alpha-helix to beta-hairpin transition. *Proteins*, **53**, 220–228.
47. Yin, S., Ding, F. & Dokholyan, N. V. (2007). Eris: an automated estimator of protein stability. *Nat. Methods*, **4**, 466–467.
48. Yin, S., Ding, F. & Dokholyan, N. V. (2007). Modeling backbone flexibility improves protein stability estimation. *Structure*, **15**, 1567–1576.
49. Galaleldeen, A., Strange, R. W., Whitson, L. J., Antonyuk, S. V., Narayana, N., Taylor, A. B. *et al.* (2009). Structural and biophysical properties of metal-free pathogenic SOD1 mutants A4V and G93A. *Arch. Biochem. Biophys.* **492**, 40–47.
50. Feig, M., Karanicolas, J. & Brooks, C. L. (2004). MMTSB Tool Set: enhanced sampling and multiscale modeling methods for applications in structural biology. *J. Mol. Grap. Model.* **22**, 377–395.
51. Kabsch, W. (1976). Solution for best rotation to relate 2 sets of vectors. *Acta Crystallogr. A*, **32**, 922–923.